Experimental Gerontology 207 (2025) 112800

Contents lists available at ScienceDirect

Experimental Gerontology

journal homepage: www.elsevier.com/locate/expgero

Dehydroacteoside rejuvenates senescence via *TVP23C-CDRT4* regulation

Yoo Jin Lee [a,1], Eun Seon Song [a,1], Yun Haeng Lee [a], Kyeong Seon Lee [b,c], Byeonghyeon So [a], Ji Ho Park [a], Jee Hee Yoon [a], Duyeol Kim [a], Minseon Kim [a], Hyung Wook Kwon [a,d], Youngjoo Byun [b,c,*], Ki Yong Lee [b,c,*], Joon Tae Park [a,d,**]

[a] Division of Life Sciences, College of Life Sciences and Bioengineering, Incheon National University, Incheon 22012, Republic of Korea
[b] College of Pharmacy, Korea University, Sejong 30019, Republic of Korea
[c] Interdisciplinary Major Program in Innovative Pharmaceutical Sciences, Korea University, Sejong 30019, Republic of Korea
[d] Convergence Research Center for Insect Vectors, Incheon National University, Incheon 22012, Republic of Korea

ARTICLE INFO

Section Editor: Anna Picca

Keywords:
Senescence rejuvenation
Dehydroacteoside
Reactive oxygen species
TVP23C-CDRT4

ABSTRACT

One of the major factors inducing senescence is reactive oxygen species (ROS) produced from dysfunctional mitochondria. Therapeutic strategies that reduce mitochondrial ROS generation are considered essential for rejuvenating senescence, but effective methods have not yet been established. Here, we screened phenylpropanoids (PPs), secondary metabolites produced in response to oxidative stress in plants, and identified dehydroacteoside as a potential candidate. Dehydroacteoside restored mitochondrial function, thereby reducing mitochondrial ROS generated by inefficient electron transport. Furthermore, senescence-associated phenotypes were restored by dehydroacteoside-mediated ROS reduction. Using RNA sequencing, we identified *TVP23C-CDRT4* as a gene that plays a critical role in dehydroacteoside-mediated senescence rejuvenation. Knockdown of *TVP23C-CDRT4* showed similar effects to dehydroacteoside, reducing ROS and subsequently restoring senescence-associated phenotypes. Taken together, our study uncovered a novel mechanism by which dehydroacteoside reduces mitochondrial ROS generation, thereby restoring senescence. Our findings open the way to a new field of anti-aging therapy aimed at controlling senescence by modulating ROS production in mitochondria.

1. Introduction

Changes in organelle function, particularly mitochondrial degeneration, are one of the most prominent hallmarks of senescence (Bolden and Lowe, 2015; Bouska et al., 2019). During senescence, mitochondria undergo structural changes, including an increase in size, which affect their function (Boffoli et al., 1994). Defective mitochondria are unable to efficiently transfer electrons in the electron transport chain (ETC), generating ROS as byproducts (Hwang et al., 2009). Defective mitochondria are one of the main sources of ROS, but they are also targets of ROS-mediated oxidative stress (Lee et al., 2023). As mitochondrial damage worsens, a vicious cycle of increasing ROS production begins (Lee et al., 2023). This leads to increased ROS levels, which in turn affect the function of the organelle, ultimately leading to senescence (Giorgi et al., 2018). The important role of ROS-induced damage in the progression of senescence is also supported by studies in a nematode model with *mev-1* (complex II homolog) mutations. *mev-1* mutants exhibit inefficient electron transport in the ETC, which leads to significantly increased ROS production (Senoo-Matsuda et al., 2001). Increased ROS levels lead to physiological changes in *mev-1* mutants, such as the accumulation of protein carbonyl derivatives and lipofuscin (Adachi et al., 1998; Hosokawa et al., 1994). Other studies on complex II also supported the link between ROS and aging. The iron chelator deferoxamine reduces complex II activity by suppressing Fe—S cluster rotation (Yoon et al., 2002). Reduced complex II activity upregulates mitochondrial ROS generation, which inhibits cell growth (Yoon et al., 2002, 2003). In addition to complex II, other studies focusing on complex IV also support this phenomenon. *Transforming growth factor beta-1* (*TGF-*

* Corresponding authors at: College of Pharmacy, Korea University, Sejong 30019, Republic of Korea.
** Correspondence to: J.T. Park, Division of Life Sciences, College of Life Sciences and Bioengineering, Incheon National University, Incheon 22012, Republic of Korea.
E-mail addresses: yjbyun1@korea.ac.kr (Y. Byun), kylee11@korea.ac.kr (K.Y. Lee), joontae.park@inu.ac.kr (J.T. Park).
[1] These authors contributed equally to this work.

https://doi.org/10.1016/j.exger.2025.112800
Received 20 March 2025; Received in revised form 16 May 2025; Accepted 2 June 2025
Available online 3 June 2025

β1) inhibits complex IV function, thereby increasing mitochondrial ROS generation. Increased oxidative stress induced by *TGF-β1* leads to degenerative outcomes (Byun et al., 2014, 2012; Yoon et al., 2005). Therefore, approaches targeting ROS generation in mitochondria may be helpful in antiaging therapies (Richards et al., 2011; Zhavoronkov et al., 2012). Given the importance of ROS-induced oxidative stress in aging, the discovery of drugs that can effectively reduce it is a top priority.

Phenylpropanoids (PPs) are a type of secondary metabolites found in plants. They are essential for a variety of physiological functions, such as pathogen defense and environmental stress responses (Korkina, 2007). The protective activity of PPs in plants is based on their peroxyl radical scavenging activity, which either scavenges oxygen species directly or breaks their chains (Korkina, 2007). PPs have recently been shown to provide many health benefits to humans. PPs are known to have antiviral, antibacterial, and antifungal activities, and its use in anticancer therapy has been actively studied recently (Neelam et al., 2020). Most of these benefits are related to the free radical chelating activities of PPs (Neelam et al., 2020). However, it remains to be elucidated whether these properties of PP can be used to control senescence.

The major organelle that generates ROS is the mitochondria (Turrens, 2003). >90 % of oxygen is used in mitochondria, and complexes in ETC converts 1–5 % of oxygen into ROS (Turrens, 2003). One of the many mitochondrial-specific dyes designed to detect mitochondrial ROS, dihydrorhodamine 123 (DHR123), has been widely used. DHR123 is produced when rhodamine 123, a dye that passively diffuses across the plasma membrane and specifically stains mitochondria, is reduced (Henderson and Chappell, 1993). When DHR123 binds to hydroxyl radicals, it is oxidized to cationic rhodamine 123, which allows measurement of mitochondrial ROS (Dickinson et al., 2010). Another mitochondrial-specific dye designed to detect mitochondrial ROS is MitoSOX. MitoSOX consists of a superoxide anion-sensitive dihydroethidium conjugate bound to a triphenylphosphonium moiety localized in the mitochondrial matrix (Kauffman et al., 2016). MitoSOX binds to superoxide anions within the mitochondrial matrix and is oxidized to cationic dihydroethidium complexes, which allows measurement of mitochondrial ROS concentrations.

Here, we demonstrate that dehydroacteoside functions as an antioxidant that reduces mitochondrial ROS generation in senescent fibroblasts. Dehydroacteoside rejuvenated senescence through reducing mitochondrial ROS generation. Furthermore, the underlying mechanism was discovered using transcriptome analysis. Here, we propose a novel anti-senescence mechanism using dehydroacteoside.

2. Materials and methods

2.1. Cell culture

This study used human dermal fibroblasts (PCS–201–010; ATCC, Manassas, VA, USA). In accordance with the protocols of earlier research, each cell was cultivated under particular media and culture conditions (Yoon et al., 2024). Human dermal fibroblasts were determined as young and senescent fibroblasts based on whether the number of cells doubled <2 days or >14 days, respectively (Cho et al., 2022; Kang et al., 2017; Yoon et al., 2018). Pre-senescent fibroblasts were identified if the cell population doubled in 5–7 days (Kim et al., 2023).

2.2. Preparation of phenylpropanoids

Dehydroacteoside and methylnissolin-3-O-β-glucoside were isolated from *Catalpa ovata*, and *Astragalus membraceus*, respectively (Park et al., 2018; Vinh et al., 2023). Coumestrol was purchased from Sigma (27885–50 MG). The structure was identified by ^{1}H–, ^{13}C NMR. ^{1}H–, ^{13}C NMR data are available in the supplementary information (Figs. S1–S6).

2.3. Flow cytometric analysis of reactive oxygen species (ROS)

Senescent fibroblasts were administered with DMSO (0.01 %), dehydroacteoside (4 μM), coumestrol (4 μM), or methylnisolone-3-O-β-glucoside (4 μM) at 4-day intervals for 12 days. Then, cells were administered with medium containing 5 μM MitoSOX (M36008; Life Technologies, Carlsbad, CA, USA) or 30 μM DHR123 (10056–1; Biotium, Fremont, CA, USA) for 30 min at 37 °C. As in our previous study, ROS was analyzed using flow cytometry (Yoon et al., 2024).

2.4. Cellular proliferation assay

Senescent fibroblasts were seeded in 96-well plates (353072; Corning, Corning, NY, USA) at a density of 1×10^3 cells per well. Senescent fibroblasts were then exposed to either DMSO (0.01 %) or dehydroacteoside (0.25, 0.5, 1, 2, or 4 μM) at 4-day intervals for 12 days. The EZ-cytox reagent (EZ-5000; DoGenBio, Seoul, Republic of Korea) was used to ca cell proliferation.

2.5. Cell viability measurement

For 12 days, the Cedex HiRes Analyzer (05650216001; Roche, Basel, Switzerland) was used to evaluate cell viability once every 4 days.

2.6. Analysis of mitochondrial membrane potential (MMP)

Senescent fibroblasts were administered with DMSO (0.01 %) or dehydroacteoside (0.5 μM) at 4-day intervals for 12 days. MMP was then evaluated using the methodology from the earlier study (Yoon et al., 2024).

2.7. Analysis of oxygen consumption rate (OCR), ATP production rate, and extracellular acidification rate (ECAR)

OCR and ATP production rates were measured using the Seahorse XF Cell Mito Stress Test Kit (101706–100; Seahorse Bioscience, Billerica, MA, USA). ECAR was measured using Seahorse XF Glycolytic Rate Assay Kit (103344–100; Seahorse Bioscience). Seahorse XFe96 analyzer (Seahorse Bioscience) was used in accordance with the manufacturer's instructions.

2.8. Immunofluorescence

According to previous methods, the immunofluorescence sample was prepared (Kang et al., 2017). Primary antibodies comprised anti-OXPHOS cocktail mouse antibody (ab110411; 1:200 dilution; abcam, Cambridge, England) and anti-LC3B rabbit antibody (A19665; 1:200 dilution; abclonal, Boston, MA, USA). Alexa Fluor® 488 goat anti-rabbit IgG antibody (A–11008; 1:200 dilution; Invitrogen, Waltham, MA, USA) and Alexa Fluor® 647 goat anti-mouse IgG antibody (A–28181; 1:200 dilution; Invitrogen) were utilized. Images were captured using a Carl Zeiss LSM 700 confocal microscope.

2.9. Analysis of autophagic flux

Senescent fibroblasts were administered with DMSO (0.01 %) or dehydroacteoside (0.5 μM) at 4-day intervals for 12 days. Then, cells were administered with (w/) or without (w/o) 20 μM chloroquine (CQ) 24 h prior to flow cytometry. After that, cells were stained for 30 min using either 500 nM LysoTracker™ Deep Red (LTDR) (L7526; Invitrogen, Waltham, MA, USA) or Cyto-ID staining solution (ENZ-51031-0050; Enzo Life Sciences, Long Island, NY, USA). MFI stands for mean fluorescence intensity. [MFI Cyto-ID (w/ CQ)/MFI LTDR (w/ CQ)] − [MFI Cyto-ID (w/o CQ)/ MFI LTDR (w/o CQ)] is the autophagic flux.

2.10. Analysis of mitochondrial mass and autofluorescence

Senescent fibroblasts were administered with DMSO (0.01 %) or dehydroacteoside (0.5 μM) at 4-day intervals for 12 days. Cells were stained for 30 min at 37 °C in a medium containing 50 nM MitoTrackerTM Deep Red FM (M46753; Invitrogen) in order to measure mitochondrial mass. Cells were stained for 30 min at 37 °C in a dye-free medium to measure autofluorescence. Then, as previously mentioned, flow cytometry analysis was carried out (Lee et al., 2022).

2.11. Neutral comet assay

A CometAssay Single Cell Gel Electrophoresis Assay Kit (4250–050–K; R&D systems, Minneapolis, MN, USA) was used to measure the length of the DNA tail. The manufacturer's guidelines were adhered to.

2.12. Quantitative polymerase chain reaction (qPCR)

As previously mentioned, qPCR was carried out (Kuk et al., 2022). For qPCR, the following primer was utilized (Table 1).

2.13. Transcriptome expression profiling

Total RNA was collected from senescent fibroblasts administered with DMSO (0.01 %) or dehydroacteoside (0.5 μM) at 4-day intervals for 12 days. The RNase Mini Kit (74,104; QIAGEN) was used to generate total RNA in accordance with the manufacturer's instructions. For transcriptome expression profiling, the procedure outlined in a prior study was followed (Kuk et al., 2025).

2.14. Preparation of shRNA

For the knockdown of *TVP23C-CDRT4*, *TVP23C-CDRT4* shRNA constructs were subcloned using the pLKO.1-puro lentiviral vector (8453; Addgene, Watertown, MA, USA) with following oligomers in Table 2. Control shRNA used the pLKO.1-puro lentiviral vector.

2.15. Lenti–viral production and infection

The virus was created using human embryonic kidney (HEK) 293 T cells (CRL-3216; ATCC). Lipofectamine 2000 (11,668,019; Invitrogen) was used to transfect HEK 293 T cells with 2.5 μg PAX2 plasmid, 2.5 μg VSV.G plasmid, and 5 μg shRNA plasmid. 24 h after transfection, viral supernatants were gathered. Polybrene (TR–1003–G; 8 μg/mL; Millipore, Burlington, MA, USA) was added to the virus production medium.

2.16. Statistical analysis

A statistical software program (GraphPad Prism 9; San Diego, CA, USA) was used to conduct the statistical analyses. The significance of the differences was assessed using the student's *t*-test and two–way ANOVA followed by Bonferroni's post–hoc test.

3. Results

3.1. Dehydroacteoside significantly decreases mitochondrial ROS levels in senescent fibroblasts

To investigate potential agents that can effectively lower mitochondrial ROS levels in senescent fibroblasts, we used dehydroacteoside, coumestrol, and methylnissolin-3-O-β-glucoside, which belong to PPs. Dehydroacteoside is an oxidized form of acteoside that has anti-inflammatory and antioxidant activities, but its function is not well understood (Kohda et al., 1989; Xiao et al., 2022). Coumestrol is a type of isoflavonoid compound with antioxidant and anti-inflammatory properties (Xu et al., 2021). Methylnissolin-3-O-β-glucoside is a flavonoid with antioxidant and anti-inflammatory activities (Wu et al., 2021).

Senescent fibroblasts were treated with the three substances at 4 μM. Then, to determine how each substance affects mitochondrial ROS levels, levels of hydroxyl radicals were assessed using DHR123 (Henderson and Chappell, 1993). Among the three agents, dehydroacteoside significantly decreased mitochondrial hydroxyl radicals compared to the DMSO control (Fig. 1A). However, coumestrol and methylnissolin-3-O-β-glucoside, which are known to have antioxidant activities, did not decrease ROS levels (Fig. 1A). We then used MitoSOX to determine how each substance affects mitochondrial ROS levels, particularly superoxide anions (Kauffman et al., 2016). All three agents did not significantly decrease mitochondrial superoxide anions compared to the DMSO control (Fig. S7). These data indicate that among the three known antioxidants, only dehydroacteoside decreased mitochondrial hydroxyl radicals.

The finding that dehydroacteoside is effective in reducing mitochondrial hydroxyl radicals led us to investigate the optimal concentration of dehydroacteoside for rejuvenating senescence. Given that cell cycle arrest is a hallmark of senescence (Poivre and Duez, 2017), we investigated whether dehydroacteoside promotes cell proliferation in senescent fibroblasts. Senescent fibroblasts were treated with dehydroacteoside at concentrations of 0.25, 0.5, 1, 2, and 4 μM. All concentrations of dehydroacteoside significantly increased cell proliferation compared to the DMSO control (Fig. 1B).

Based on the observation that dehydroacteoside exhibited diverse effects on cell proliferation over a wide concentration range (0.25–4 μM), we investigated the effects of dehydrolacteoside on mitochondrial ROS levels over a wide concentration range (0.25–4 μM) using DHR123. At concentrations of 0.25 μg/mL, dehydroacteoside did not affect mitochondrial hydroxyl radicals compared to the DMSO control (Fig. 1C). In contrast, at a concentration of 0.5 and 4 μg/mL, dehydroacteoside significantly decreased mitochondrial hydroxyl radicals compared to the DMSO control (Fig. 1C). However, when senescent fibroblasts were administered with dehydroacteoside at concentrations of 1 and 2 μg/mL, the ROS effect was not significantly decreased (Fig. 1C).

Table 1
Details of primers used in qPCR.

Target	Orientation	Sequence (5′–3′)	Size (bp)
36B4 (accession number: NM_053275)	Forward	CAGCAAGTGGGAAGGTGTAATCC	23
	Reverse	CCCATTCTATCATCAACGGGTACAA	25
TGF-β1 (accession number: NM_000660.7)	Forward	AGCTGTACCAGAAATACAGCAACAAT	26
	Reverse	CCGGTGACATCAAAAGATAACCAC	24
IL–8 (accession number: NM_000584.4)	Forward	CTGGCCGTGGCTCTCTTG	18
	Reverse	CCTTGGCAAAACTGCACCTT	20
Procollagen type I (accession number: NM_002593.4)	Forward	CAGACTGGCAACCTGAAGAAGTC	23
	Reverse	TCGCCCCTGAGCTCGAT	17
SLIT2 (accession number: NM_004787.4)	Forward	CAGAGCTTCAGCAACATGACCC	22
	Reverse	GAAAGCACCTTCAGGCACAACAG	23
TVP23C-CDRT4 (accession number: NM_001204478.2)	Forward	CTTGTTGTTGTCGTGTGA	18
	Reverse	CCCAATGGCTCTTTCC	16

Table 2
Details of primers used in making *TVP23C-CDRT4* shRNA.

Target	Orientation	Sequence (5′–3′)	Size (bp)
TVP23C-CDRT4 (1)	Forward	CCGGTTGCTCAGCAGCAGCTTTATTTCAAGAGAATAAAGCTGCTGCTGAGCAATTTTTG	59
	Reverse	AATTCAAAAATTGCTCAGCAGCAGCTTTATTCTCTTGAAATAAAGCTGCTGCTGAGCAA	59
TVP23C-CDRT4 (2)	Forward	CCGGGAGTCCTCTCAAGAGAATAAATCAAGAGTTTATTCTCTTGAGAGGACTCTTTTTG	59
	Reverse	AATTCAAAAAGAGTCCTCTCAAGAGAATAAACTCTTGATTTATTCTCTTGAGAGGACTC	59

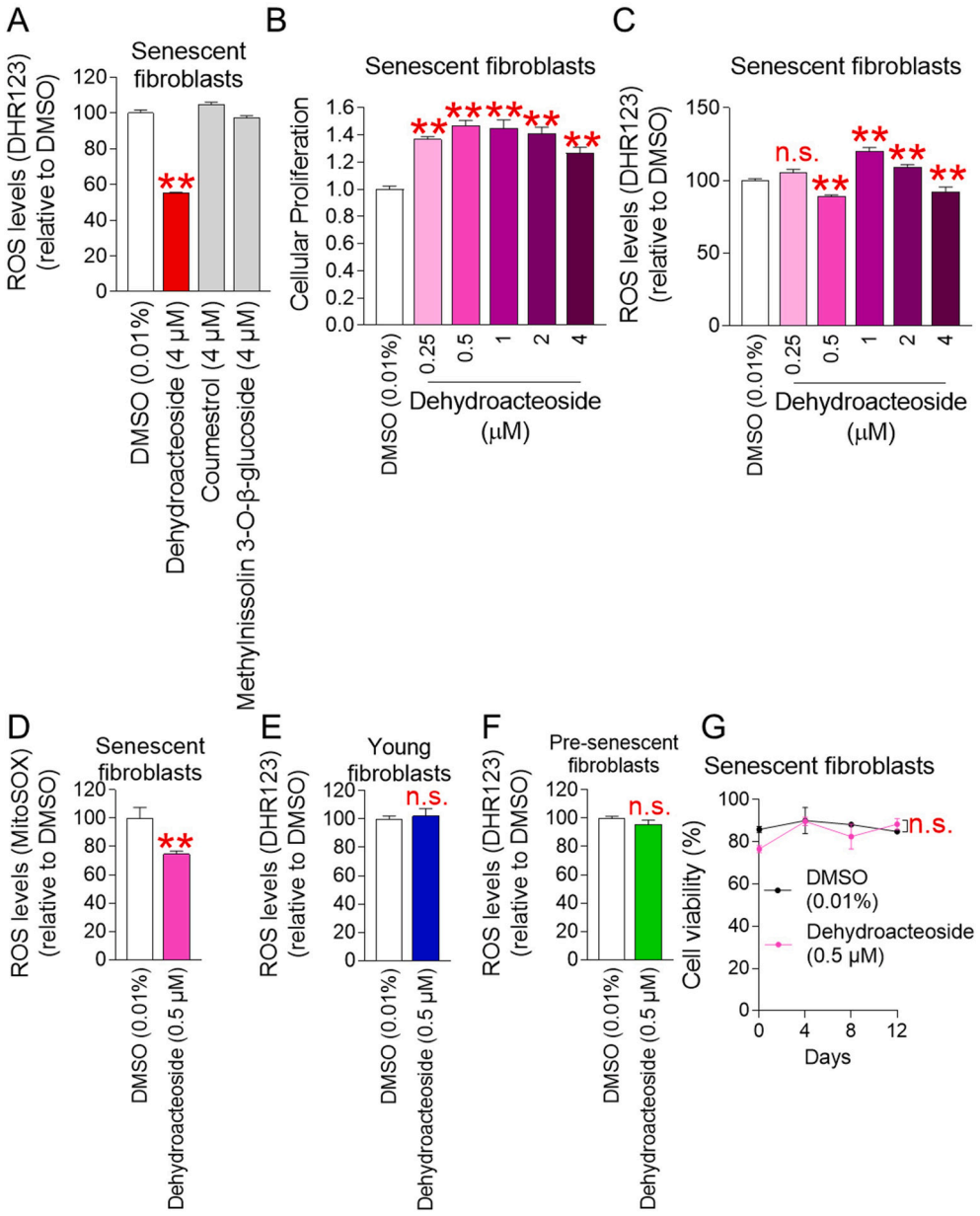

Fig. 1. Dehydroacteoside significantly decreases mitochondrial ROS levels in senescent fibroblasts. (A) Senescent fibroblasts were administered with DMSO (0.01 %), dehydroacteoside (4 μM), coumestrol (4 μM), or methylnissolin-3-O-β-glucoside (4 μM) at 4-day intervals for 12 days. Use of dihydrorhodamine 123 (DHR123) for flow cytometry. **P < 0.01, Student's *t*–test. Mean ± S.D., n = 3. (B and C) Senescent fibroblasts were administered with DMSO (0.01 %) or different concentrations of dehydroacteoside (0.25, 0.5, 1, 2, and 4 μM) at 4-day intervals for 12 days. Then, cellular proliferation was evaluated using EZ-cytox reagent (B) and mitochondrial ROS was evaluated using DHR123 (C). **P < 0.01, Student's *t*–test. Mean ± S.D., n = 6. (D, E, and F) Senescent, young, or pre-senescent fibroblasts were administered with DMSO (0.01 %) or dehydroacteoside (0.5 μM) at 4-day intervals for 12 days. Use of DHR123 for flow cytometry. **P < 0.01, Student's *t*–test. Mean ± S.D., n = 3. (G) Senescent fibroblasts were administered with DMSO (0.01 %) or dehydroacteoside (0.5 μM) at 4-day intervals for 12 days. Assessment of cell viability following treatment for 0, 4, 8, and 12 days. n.s. (not significant), two–way ANOVA followed by Bonferroni's post–hoc test. Mean ± S.D., n = 3.

The reason for these outcomes could be that the dehydroacteoside concentrations (0.25, 1, and 2 μg/mL) did not fall within the ideal range to achieve the mitochondrial ROS–reducing effect (Sweeney, 1983). Therefore, a concentration of 0.5 μM was determined to be the optimal concentration as it induced the greatest cell proliferation and the greatest decrease in mitochondrial hydroxyl radicals.

The optimal concentration of dehydroacteoside (0.5 μM) did not match the concentration used in screening (4 μM). In addition, 4 μM dehydroacteoside only decreased hydroxyl radicals, but not superoxide anion (Figs. 1A and S7). Because we found that 0.5 μM dehydroacteoside decreased hydroxyl radicals (Fig. 1C), we investigated the effect of 0.5 μM dehydroacteoside on superoxide anion. Treatment with dehydroacteoside at 0.5 μM significantly decreased superoxide anions compared to the DMSO control (Fig. 1D). These results indicate that the mitochondrial ROS–reducing effect of dehydroacteoside was maintained even at 0.5 μM.

Our findings that dehydroacteoside lowers mitochondrial ROS in senescent fibroblasts raised the question of whether it had the same beneficial effect on young and pre-senescent fibroblasts. Therefore, we checked whether dehydroacteosides showed the same ROS-reducing effect in young and pre-senescent fibroblasts. Dehydroacteoside did not exhibit mitochondrial ROS-reducing effects in young and pre-senescent fibroblasts, as was seen in senescent fibroblasts (Fig. 1E and F). Taken together, these results suggest that the mitochondrial ROS-reducing effect of dehydroacteoside is limited to senescent fibroblasts, further enhancing the potential of dehydroacteoside as a therapeutic for aging.

Next, we investigated the toxicity of dehydroacteoside at the selected concentrations by examining cell viability. Dehydroacteoside is not cytotoxic at the selected concentration, as evidenced by the similar viability of senescent fibroblasts treated with 0.5 μM dehydroacteoside and fibroblasts treated with DMSO (Fig. 1G).

3.2. Dehydroacteoside restores mitochondrial function

Ineffective electron transport in the ETC is a primary cause of ROS generation in the mitochondria (Turrens, 2003). Superoxide radicals are produced by ETC components due to inefficient electron transport (Turrens, 2003). The most prominent ROS-induced mitochondrial damage is a decrease in mitochondrial membrane potential (MMP), which arises from the movement of protons between the mitochondrial matrix and mitochondrial intermembrane space (Sherratt, 1991). Therefore, ineffective electron transport raises mitochondrial ROS generation and lowers MMP, while effective electron transport lowers mitochondrial ROS generation and raises MMP (Miwa et al., 2022). Because we found that mitochondrial ROS levels were decreased by dehydroacteoside, we evaluated the effect of dehydroacteoside on MMP. In senescent fibroblasts treated with dehydroacteoside, MMP was significantly increased compared to the DMSO control (Fig. 2A).

MMP is a proton motive force that promotes ATP production by OXPHOS (Mitchell and Moyle, 1967). Young fibroblasts ATP production via OXPHOS and reduce the dependence on glycolysis, but senescent fibroblasts become more dependent on glycolysis due to mitochondrial dysfunction (Lee et al., 2021). Because we found that MMP was increased by dehydroacteoside, mitochondrial metabolism, an indicator of mitochondrial function, was evaluated. The efficiency of OXPHOS and glycolysis was determined by measuring the oxygen consumption rate (OCR) and extracellular acidification rate (ECAR), respectively (Plitzko and Loesgen, 2018). Oligomycin, and carbonyl cyanide-*p*-trifluoromethoxyphenylhydrazone (FCCP), and rotenone/antimycin A were used to measure OCR (Mookerjee et al., 2017). Specifically, OCR was used to evaluate non-mitochondrial respiration (after oligomycin treatment), maximal respiration (after FCCP treatment), and ATP-coupled respiration (after rotenone/antimycin A treatment). When compared to DMSO control, dehydroacteoside administration significantly raised OCR values, indicating that it boosted non-mitochondrial respiration, maximum respiration, and ATP-coupled respiration (Fig. 2B; black vs. pink lines). Then, rotenone/antimycin A and 2-deoxy-D-glucose (2-DG) were used to measure ECAR (Plitzko and Loesgen, 2018). Specifically, ECAR was used to evaluate the basal glycolysis rate (before rotenone/antimycin A treatment), compensatory glycolysis rate (after rotenone/antimycin A treatment), and post-2-DG acidification

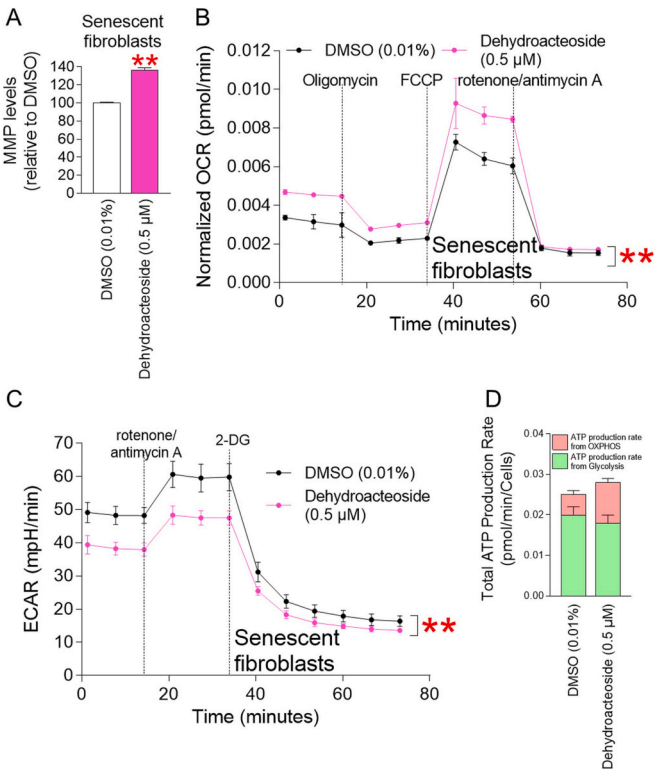

Fig. 2. Dehydroacteoside restores mitochondrial function. (A) Senescent fibroblasts were administered with DMSO (0.01 %) or dehydroacteoside (0.5 μM) at 4-day intervals for 12 days. Mitochondrial membrane potential (MMP) was evaluated using JC-10. **P < 0.01, Student's *t*–test. Mean ± S.D., n = 3. (B and C) Measurement of oxygen consumption rate (OCR; pmol/min) and extracellular acidification rate (ECAR; mpH/min) after 12 days of treatment with DMSO (0.01 %) or dehydroacteoside (0.5 μM) (black line: DMSO–treated senescent fibroblasts, pink line: dehydroacteoside–treated senescent fibroblasts). **P < 0.01, two–way ANOVA followed by Bonferroni's post–hoc test. Means ± S.D., n = 3. (D) Assessment of total ATP production rate after 12 days of treatment with DMSO (0.01 %) or dehydroacteoside (0.5 μM). Pink square indicates the ATP production rate from OXPHOS. Green square indicates that ATP production rate from glycolysis. Mean ± S.D., n = 3. (For interpretation of the references to color in this figure legend, the reader is referred to the web version of this article.)

(after 2-DG treatment). When compared to DMSO control, dehydroacteoside administration significantly lowered ECAR values, indicating that it lowered basal glycolysis rate, compensatory glycolysis rate, and post-2-DG acidification (Fig. 2C; black vs. pink lines). To verify these results, we measured the ratio of ATP production by OXPHOS and glycolysis. Dehydroacteoside enhanced the efficiency of OXPHOS, as evidenced by increased ATP production by OXPHOS and decreased ATP production by glycolysis (Fig. 2D). These results indicate that efficient electron transport by dehydroacteoside is a unique mechanism by which it reduces mitochondrial ROS production, as higher OXPHOS efficiency suggests efficient electron transport.

3.3. Dehydroacteoside eliminates dysfunctional mitochondria through mitophagy

The finding of mitochondrial functional recovery by dehydroacteoside prompted us to identify the mechanism by which dysfunctional mitochondria are removed in senescent fibroblasts. Since mitophagy removes damaged mitochondria and preserves healthy mitochondrial function (Picca et al., 2023), we hypothesized that dehydroacteoside removes dysfunctional mitochondria by activating mitophagy. We therefore investigated the effects of dehydroacteoside on mitophagy.

Since dysfunctional mitochondria are removed by autophagosomes (Wang and Klionsky, 2011), mitophagy was examined through observing whether autophagosomal membrane protein microtubule-associated protein 1 A/1B-light chain 3B (LC3B) and mitochondria colocalize (Hanna et al., 2012). In senescent fibroblasts treated with DMSO, colocalization of LC3B and mitochondria was barely observed (Fig. 3A; white arrows). However, colocalization reappeared after senescent fibroblasts were treated with dehydroacteoside (Fig. 3A; white arrows). To confirm the role of dehydroacteoside in mitophagy, cells were co-treated with chloroquine (CQ), which limits autophagic flux by disrupting lysosomal pH (Shintani and Klionsky, 2004). As expected, co-treatment with CQ increased autophagosome accumulation (LC3B, green) (Fig. 3B). In addition, co-treatment with CQ increased the co-localization in the dehydroacteoside-treated group compared to the DMSO-treated group (Fig. 3B; white arrows). The increased colocalization in dehydroacteoside-treated senescent fibroblasts was accompanied by significant increase of autophagic flux and decrease of mitochondrial mass, indicating that dehydroacteoside promotes mitophagy activation (Fig. 3C and D).

3.4. Dehydroacteoside ameliorates senescence-associated phenotypes

One of the prerequisites for improving senescence is restoration of mitochondrial function (Kim et al., 2019; Kuk et al., 2023; Lee et al., 2022, 2021; Park et al., 2022). The discovery of restoration of mitochondrial function by dehydroacteoside led to evaluate the effect of dehydroacteoside on senescence. ROS directly damage DNA or indirectly damage DNA by deteriorating proteins involved in DNA maintenance (Checa and Aran, 2020). Since we found a decrease in mitochondrial ROS generation by dehydroacteoside, we examined the effect of dehydroacteoside on DNA damage. To measure the presence of DNA damage, DNA double-strand breaks (DSBs) were examined [50]. Senescent fibroblasts administered with dehydroacteoside showed a significant decrease in DNA DSBs compared to the DMSO control suggesting a decrease in DNA damage by dehydroacteoside (Fig. 4A).

Subsequently, autofluorescence levels were measured to assess the amount of lipofuscin, a key feature of senescence (Ilie et al., 2020). After dehydroacteoside treatment, autofluorescence levels were significantly reduced, indicating that dehydroacteoside reduced lipofuscin levels (Fig. 4B).

Cytokines and chemokine secreted by senescent cells are referred to

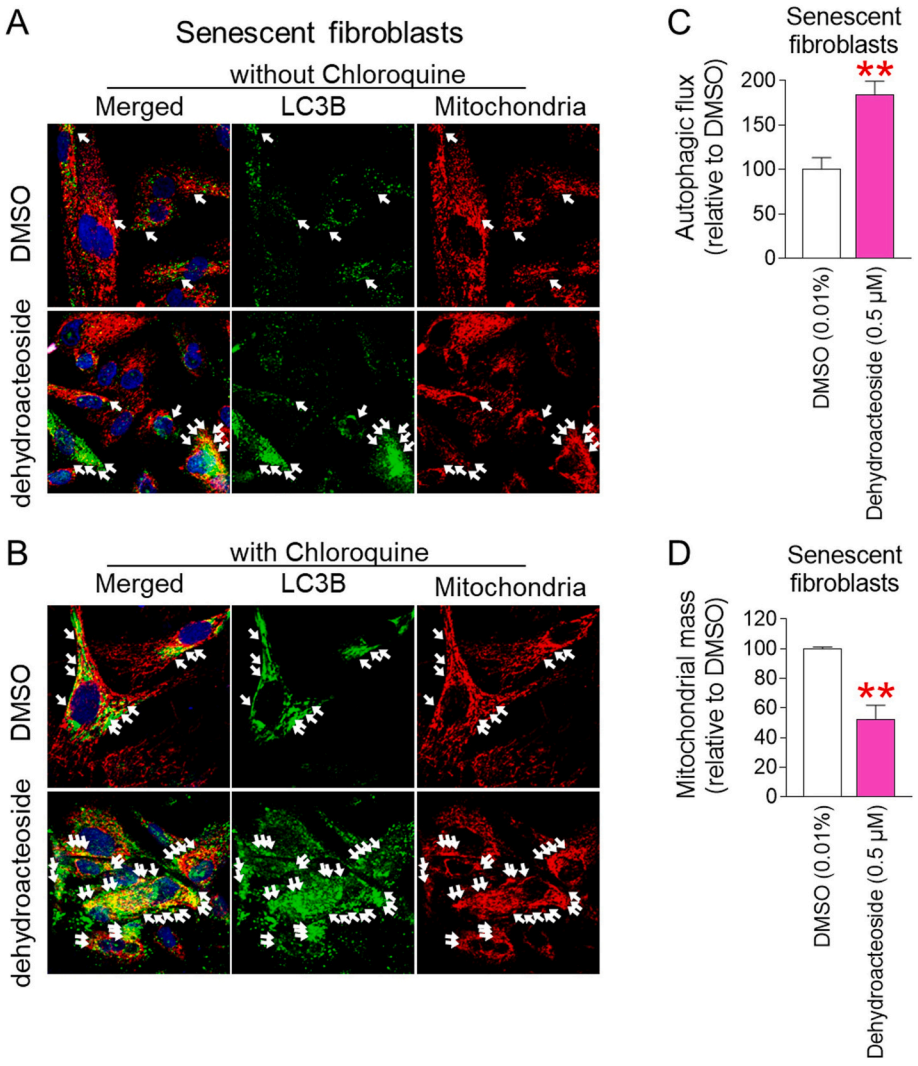

Fig. 3. Dehydroacteoside eliminates dysfunctional mitochondria through mitophagy. (A and B) Senescent fibroblasts were treated with DMSO (0.01 %) or dehydroacteoside (0.5 μM) for 12 days. Immunostaining for LC3B (green) and mitochondria (red) without chloroquine (A) or with chloroquine treatment (B). Scale bar 10 μm. White arrow indicates mitophagy. (C and D) Measurement of autophagic flux (C) and mitochondrial mass (D) after 12 days of treatment with DMSO (0.01 %) or dehydroacteoside (0.5 μM). **P < 0.01, Student's *t*–test. Mean ± S.D., n = 3. (For interpretation of the references to color in this figure legend, the reader is referred to the web version of this article.)

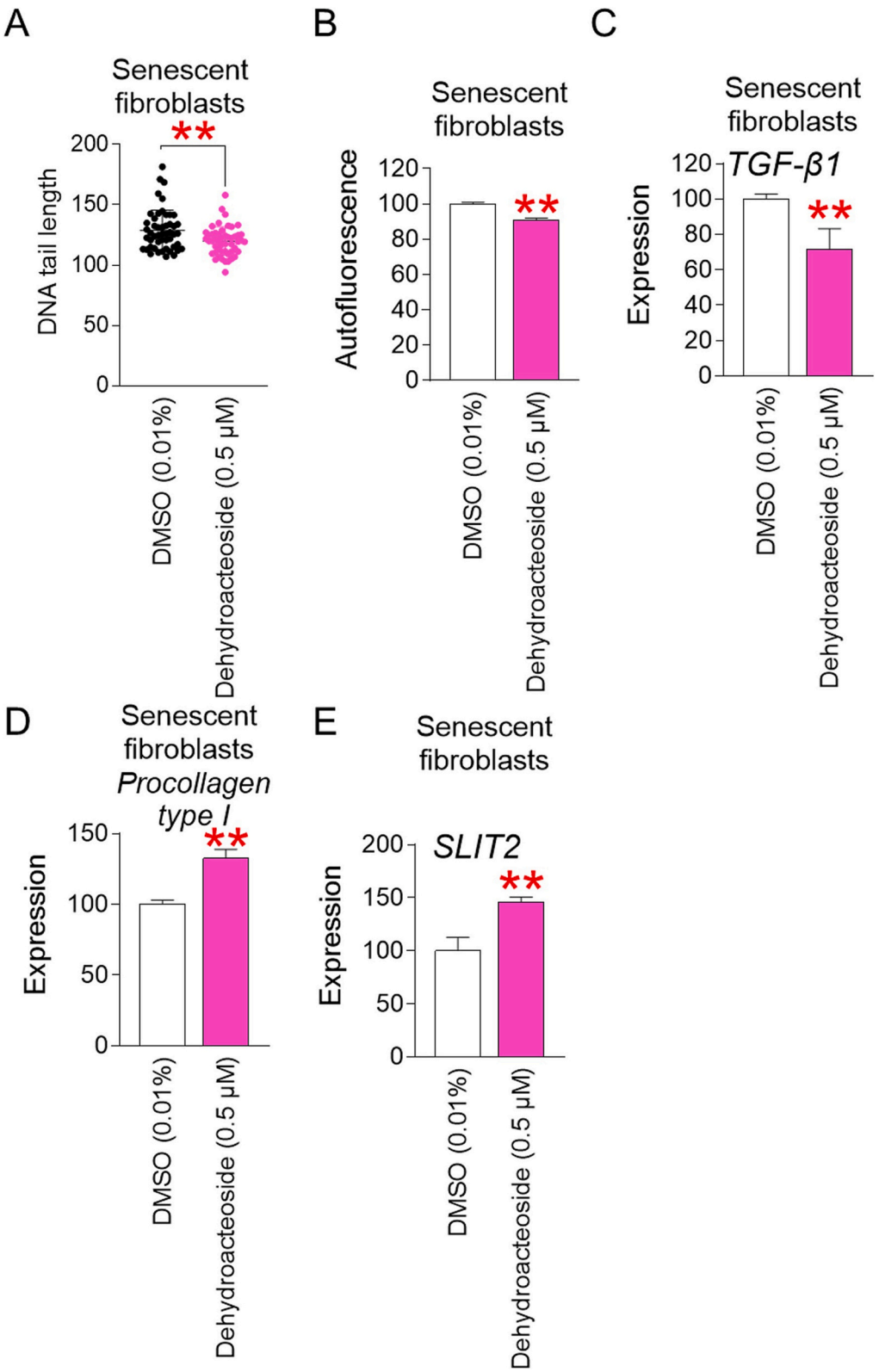

Fig. 4. Dehydroacteoside ameliorates senescence-associated phenotypes. (A) DNA tail length was measured after 12 days of treatment with DMSO (0.01 %) or dehydroacteoside (0.5 μM). A DNA tail's length is represented by each dot. **P < 0.01, Student's t–test. Mean ± S.D., n = 50. (B) After 12 days of treatment with DMSO (0.01 %) or dehydroacteoside (0.5 μM) in senescent fibroblasts, autofluorescence levels were evaluated. **P < 0.01, Student's *t*–test. Mean ± S.D., n = 3. (C) After 12 days of treatment with DMSO (0.01 %) or dehydroacteoside (0.5 μM) in senescent fibroblasts, expression levels of *TGF-β1* were evaluated. **P < 0.01, Student's *t*–test. Mean ± S.D., n = 3. (D) After 12 days of treatment with DMSO (0.01 %) or dehydroacteoside (0.5 μM) in senescent fibroblasts, expression levels of *procollagen type I* were evaluated. **P < 0.01, Student's *t*–test. Mean ± S.D., n = 3. (D) After 12 days of treatment with DMSO (0.01 %) or dehydroacteoside (0.5 μM) in senescent fibroblasts, expression levels of *SLIT2* were evaluated. **P < 0.01, Student's *t*–test. Mean ± S.D., n = 3.

as the senescence-associated secretory phenotype (SASP) (González-Gualda et al., 2021). Hydrogen peroxide is generated when ROS in the mitochondrial matrix interact with mitochondrial superoxide dismutase (Palma et al., 2020). Then, hydrogen peroxide penetrates the mitochondrial outer membrane and cause damage to cytosolic proteins, which triggers the release of SASP (IL-8, IL-6, TGF-β1, etc.) (Ichimura et al., 2003; Naik and Dixit, 2011; Nelson et al., 2018). To examine the role of dehydroacteoside on the expression of *TGF-β1*, an inflammatory SASP (Tominaga and Suzuki, 2019), dehydroacteoside was treated to senescent fibroblasts. Compared with the DMSO control, dehydroacteoside significantly reduced *TGF-β1* expression in senescent fibroblasts, suggesting downregulation of the inflammatory SASP (Fig. 4C).

Reduced collagen protein production is a hallmark of skin aging, resulting in a loss of structural support and a deterioration in the function of the skin barrier (Quan and Fisher, 2015). Specifically, in photodamaged human skin, expression of procollagen type I is reduced due to increased degradation by metalloproteinases (Varani et al., 2001). Senescent fibroblasts were treated with dehydroacteoside in order to investigate its effect on *procollagen type I* expression. Dehydroacteoside significantly upregulated *procollagen type I* expression as compared to the DMSO control, suggesting that the skin barrier's structural support has been restored (Fig. 4D).

Slit guidance ligand 2 (*SLIT2*) aids in the regeneration of skin tissue by controlling cell-cell connections (Kim et al., 2023; Qi et al., 2014). Downregulation of *SLIT2* expression compromises the function of the epidermal barrier through decreasing tissue regeneration ability (Kim et al., 2023; Wu et al., 2017). Dehydroacteoside was treated to senescent fibroblasts in order to investigate its effect on *SLIT2* expression. Dehydroacteoside significantly upregulated *SLIT2* expression, suggesting that it stimulates skin regeneration (Fig. 4E).

3.5. RNA sequencing identifies TVP23C-CDRT4 as a key regulator of senescence-ameliorating mechanisms

The discovery that dehydroacteoside has an anti-senescence effect prompted us to identify the mechanism by which dehydroacteoside rejuvenates senescence. To clarify the fundamental mechanism, we performed RNA sequencing after treating senescent fibroblasts with DMSO or dehydroacteoside. Transcriptome sequencing data were used to assess differentially expressed genes (DEG). 55 genes were significantly altered by more than two fold, according to DEG analysis (dehydroacteoside group versus DMSO group) (Blue dot; Table S1 and Fig. 5A). Among the 55 genes, *TVP23C-CDRT4* was selected as a key gene because it showed the most change (Red dot; 35-fold decrease compared to DMSO control; Table S1 and Fig. 5A).

TVP23C-CDRT4 is a naturally occurring read-through transcript between neighboring *TVP23C* (trans-Golgi network vesicle protein 23 homolog) and *CDRT4* (CMT1A duplicated region transcript 4) (Lieburg-Apers et al., 2015). Quantitative PCR found that the expression of *TVP23C-CDRT4* was significantly reduced in the dehydroacteoside-treated group compared to DMSO (Fig. 5B). Therefore, *TVP23C-CDRT4* was chosen as a key gene for dehydroacteoside-mediated senescence rejuvenation.

3.6. TVP23C-CDRT4 knockdown lowers mitochondrial ROS levels and restores senescence-associated phenotypes

The discovery that *TVP23C-CDRT4* is a key candidate for the senescence rejuvenation by dehydroacteoside prompted us to investigate whether knockdown of *TVP23C-CDRT4* could achieve the similar anti-senescence effect to dehydroacteoside. Specifically, after establishing a lentiviral system to knockdown *TVP23C-CDRT4*, senescent fibroblasts were infected with lentivirus expressing shRNA targeting *TVP23C-CDRT4* or expressing control shRNA. Compared with the control shRNA group, *TVP23C-CDRT4* shRNA group exhibited a significant reduction in *TVP23C-CDRT4* expression, indicating efficient shRNA-induced *TVP23C-CDRT4* knockdown (Fig. 6A).

Next, we investigated the effect of *TVP23C-CDRT4* knockdown on mitochondrial ROS levels. *TVP23C-CDRT4* knockdown had the similar ROS-reducing effect to dehydroacteoside, as evidenced by significantly lower mitochondrial ROS levels in *TVP23C-CDRT4* shRNA group compared to the control shRNA group (Fig. 6B).

We then examined effects of *TVP23C-CDRT4* knockdown on mitochondrial mass because ROS-induced mitochondrial dysfunction leads to an increase in mitochondrial mass as a feedback mechanism (Lee

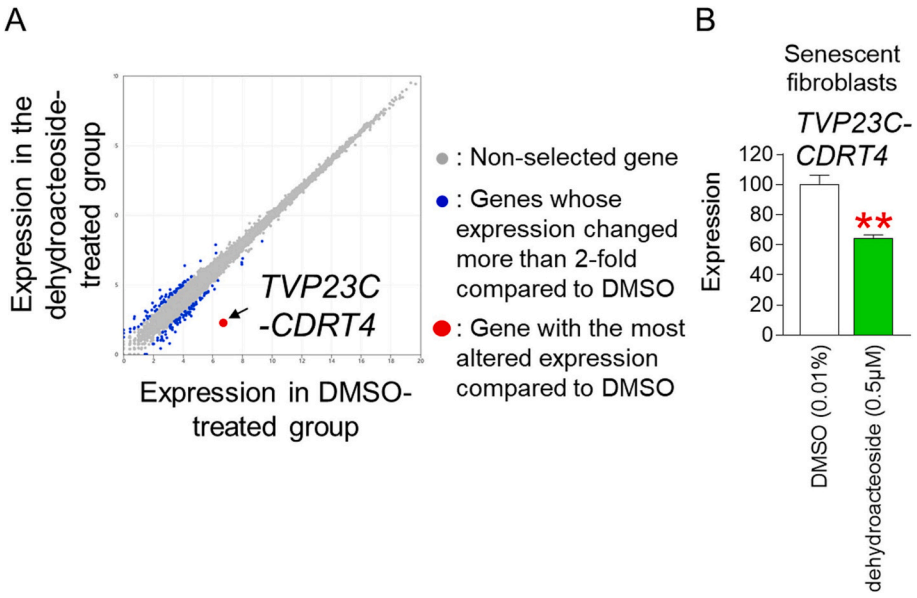

Fig. 5. RNA sequencing identifies *TVP23C-CDRT4* as a key regulator of senescence. (A) DEG analysis identified that 55 genes were significantly altered more than two fold compared to the DMSO control (blue dot). Among the 55 genes, TVP23C-CDRT4 was selected as a key candidate because it showed the most changes (red dot). Gray dot: non-selected gene. (B) After 12 days of treatment with DMSO (0.01 %) or dehydroacteoside (0.5 μM) in senescent fibroblasts, expression levels of *TVP23C-CDRT4* were examined. **P < 0.01, Student's *t*–test. Mean ± S.D., n = 3. (For interpretation of the references to color in this figure legend, the reader is referred to the web version of this article.)

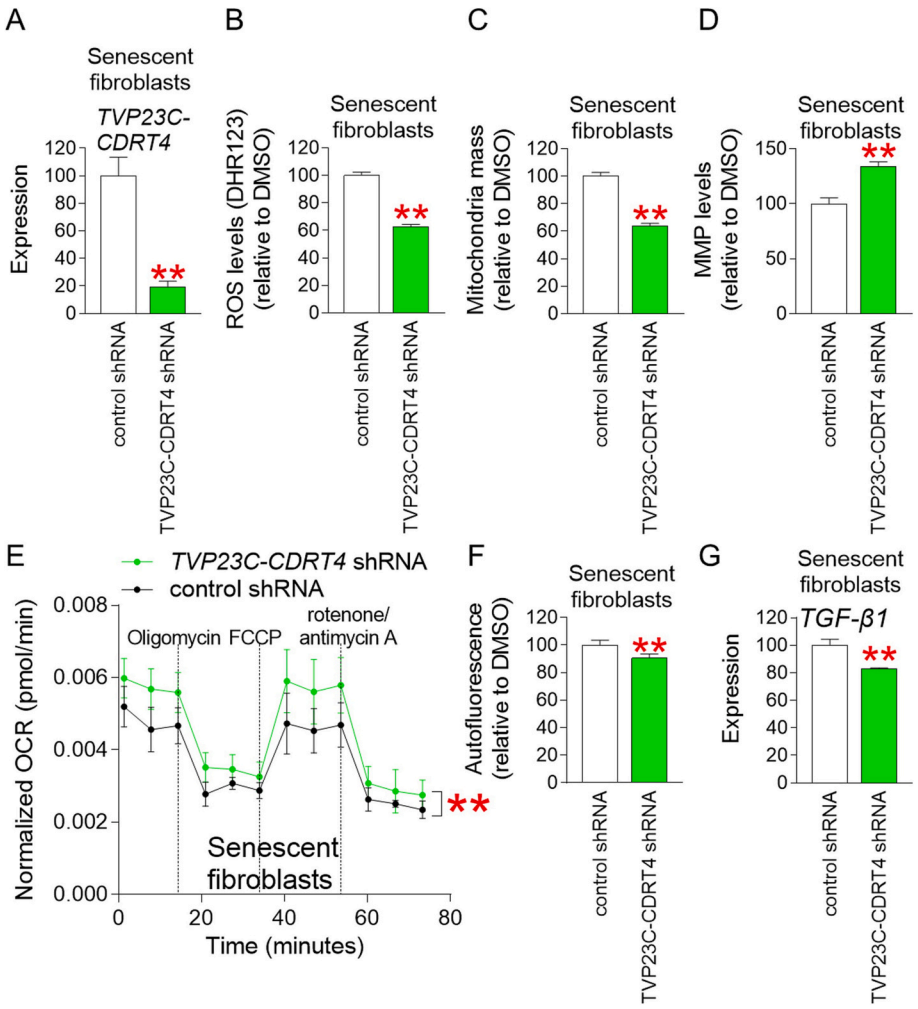

Fig. 6. *TVP23C-CDRT4* knockdown lowers mitochondrial ROS levels and restores senescence-associated phenotypes. (A) Compared with the control group, *TVP23C-CDRT4* shRNA group showed a significant decrease in *TVP23C-CDRT4* expression. **P < 0.01, Student's *t*–test. Means ± S.D., n = 3. (B) Compared with the control group, *TVP23C-CDRT4* shRNA group showed a significant decrease in mitochondrial ROS levels. **P < 0.01, Student's *t*–test. Means ± S.D., n = 3. (C) Compared with the control group, *TVP23C-CDRT4* shRNA group showed a significant decrease in mitochondrial mass. **P < 0.01, Student's *t*–test. Means ± S.D., n = 3. (D) Compared with the control group, *TVP23C-CDRT4* shRNA group showed a significant increase in MMP levels. **P < 0.01, Student's *t*–test. Means ± S.D., n = 3. (E) Compared with the control group, *TVP23C-CDRT4* shRNA group showed a significant increase in OCR values. (black line: control shRNA–transduced senescent fibroblasts, green line: *TVP23C-CDRT4* shRNA–transduced senescent fibroblasts). **P < 0.01, two–way ANOVA followed by Bonferroni's post–hoc test. Means ± S.D., n = 3. (F) Compared with the control group, *TVP23C-CDRT4* shRNA group showed a significant decrease in autofluorescence. **P < 0.01, Student's *t*–test. Means ± S.D., n = 3. (G) Compared with the control group, *TVP23C-CDRT4* shRNA group showed a significant decrease in the expression of *TGF-β1*. **P < 0.01, Student's *t*–test. Means ± S.D., n = 3. (For interpretation of the references to color in this figure legend, the reader is referred to the web version of this article.)

et al., 2002; Passos et al., 2007), *TVP23C-CDRT4* shRNA group exhibited a significant reduction in mitochondrial mass when compared to the control shRNA group (Fig. 6C). These data suggest that *TVP23C-CDRT4* knockdown had an impact similar to that of dehydroacteoside in reducing mitochondrial mass.

Next, we investigated whether mitochondrial MMP was impacted by *TVP23C-CDRT4* knockdown. MMP levels significantly increased in *TVP23C-CDRT4* shRNA group compared to the control group, suggesting that *TVP23C-CDRT4* knockdown restored mitochondrial function (Fig. 6D).

Since dehydroacteoside increased OXPHOS efficiency, we investigated whether *TVP23C-CDRT4* knockdown also increased OXPHOS efficiency. When compared to the control group, *TVP23C-CDRT4* knockdown significantly raised OCR values, indicating that it also boosted non-mitochondrial respiration, maximum respiration, and ATP-coupled respiration (Fig. 6E; black vs. green lines).

We then investigated the effects of *TVP23C-CDRT4* knockdown on autofluorescence, one of the key hallmarks of senescence (Ilie et al., 2020). *TVP23C-CDRT4* knockdown had the same autofluorescence-reducing effect as dehydroacteoside, as evidenced by the significant decrease in autofluorescence observed in *TVP23C-CDRT4* shRNA group compared to the control group (Fig. 6F).

Finally, we investigated the effects of *TVP23C-CDRT4* knockdown on the expression of *TGF-β1*, an inflammatory SASP (Tominaga and Suzuki, 2019). *TVP23C-CDRT4* knockdown had the same *TGF-β1*-reducing effect as dehydroacteoside, as evidenced by the significant decrease in the expression observed in *TVP23C-CDRT4* shRNA group compared to the control group (Fig. 6G).

4. Discussion

Mitochondria are the organelles that generate approximately 90 % of ROS (Tirichen et al., 2021). About 1–5 % of the oxygen consumed by mitochondria is converted to superoxide anions by the complexes in mitochondrial ETC (Turrens, 2003). In particular, oxygen is converted to superoxide anions by complexes I and III in the mitochondrial matrix. In addition, superoxide anions are generated by complex III in the mitochondrial intermembrane space. Dysfunctional mitochondria decrease

the activities of all complexes of the ETC (Choksi et al., 2004, 2008). Low complex I activity prevents efficient electron transfer and increases electron leakage to oxygen, resulting in faster generation of superoxide anions (Nakai and Tsuruta, 2021). When ROS generated in mitochondria damages the ETC, a vicious cycle of increased ROS generation in mitochondria begins (Lee et al., 2023). As a result of this vicious cycle, cellular organelles are damaged, their function deteriorates, and ultimately senescence occurs (Stout and Birch-Machin, 2019). These causal relationships emphasize that reducing ROS generation in mitochondria is a crucial strategy to rejuvenate senescence (Lee et al., 2023). In this study, we discovered a novel mechanism that dehydroacteoside lowers the ROS generation in the mitochondria by restoring mitochondrial function. The increase in MMP by dehydroacteoside indicates an increase in proton transport, which suggests efficient electron transport within the ETC (Nolfi-Donegan et al., 2020). Dehydroacteoside-mediated effective electron transport reduces electron leakage to oxygen, which lowers the generation of ROS as a byproduct (Zhao et al., 2019). Furthermore, we found that dehydroacteoside reduces the dependence on glycolysis as an energy source, suggesting that dehydroacteoside restores mitochondrial function. Here, we find that dehydroacteoside ameliorates senescence by a novel mechanism that reduces mitochondrial ROS generation. We propose that this novel mechanism could be an important step toward developing anti-aging therapies.

PPs are a relatively simple secondary metabolite derived from the shikimic acid pathway via phenylalanine and tyrosine in some plants (Zhu et al., 2024). PPs can be classified into five groups including flavonoids, lignins, phenols, stilbenes, and coumarins (Agar and Cankaya, 2020). Dehydroacteoside, coumestrol, and methylnissolin-3-O-β-glucoside used in this experiment also belong to PPs. Dehydroacteoside has glucose and arabinose as substituents on a phenylpropanoid backbone with hydroxyl and methoxy groups (Zhou et al., 2020). Coumestrol is a type of isoflavonoid with hydroxy substituents at positions 3 and 9 (Bickoff et al., 1964). Methylnissolin-3-O-β-D-glucoside has an isoflavonoid backbone with a methoxy group and multiple hydroxyl groups (Choi et al., 2025). All three PPs have been shown to provide anti-inflammatory and antioxidant effects by reducing cytokine expression (Castro et al., 2025; Choi et al., 2025; Muhtar et al., 2024). In this study, we evaluated the ability of these three PPs to reduce mitochondrial ROS. Among the three PPs, only dehydroacteoside showed a significant inhibitory effect on mitochondrial ROS production. This is because dehydroacteoside has distinct structural features compared with coumestrol and methylnissolin-3-O-β-D-glucoside. When dehydroacteoside and coumestrol were compared, only dehydroacteoside had a methoxy group, which could increase the overall electron density of the molecule and enhance the reaction with ROS (Van den Worm et al., 2001). Therefore, dehydroacteoside showed a higher antioxidant effect than coumestrol, which does not have a methoxy group. When comparing dehydroacteoside and methylnissolin-3-O-β-D-glucoside, both agents had sugar residues, which could directly react with ROS through the electrons of the hydroxyl group attached to the sugar (Liemburg-Apers et al., 2015). Therefore, dehydroacteoside with two sugar residues had a greater antioxidant capacity than methylnissolin-3-O-β-D-glucoside with one sugar residue. In summary, our results show that the antioxidant effect of PPs varies depending on the number of sugar molecules and the type of functional group. We suggest that further modification of dehydroacteoside may further increase the antioxidant effect. However, we acknowledge that more experiments are needed to prove this hypothesis.

TVP23C-CDRT4 is a naturally occurring read-through transcript located between neighboring TVP23C and CDRT4 on chromosome 17 (Zody et al., 2006). In a recent study, TVP23C-CDRT4 was found to be highly expressed in tissues obtained from adenoid cystic carcinoma (ACC), suggesting that it may be a potential target for ACC therapy (Tang et al., 2023). Additionally, TVP23C-CDRT4 is found at a high rate in amyotrophic lateral sclerosis, a neurodegenerative disease, and has been identified as one of the important risk factors for developing amyotrophic lateral sclerosis (Raghav et al., 2024). However, no study has investigated the role of TVP23C-CDRT4 in the progression and development of senescence. In this study, we found that dehydroacteoside improves senescence-associated phenotypes through downregulating *TVP23C-CDRT4* expression. Extending the relevance of these results, we found that similar to dehydroacteoside treatment, downregulation of *TVP23C-CDRT4* in senescent fibroblasts reduced mitochondrial ROS levels and subsequently restored senescence-associated phenotypes. Furthermore, we found that regulation of *TVP23C-CDRT4* may be one of the potential means to achieve similar effects of dehydroacteoside on senescence. Future studies should focus on exploring the mechanism by which *TVP23C-CDRT4* controls mitochondrial ROS levels.

ROS above the pathological concentration range causes an imbalance in the body's antioxidant system, which maintains the unstable structure of ROS. Excessive ROS causes permanent damage to DNA, RNA proteins, and lipids in the process of stabilizing the unstable structure (Prousek, 2007). In particular, accumulation of ROS-mediated damage induces p53 signaling dysfunction, leading to long-term cell cycle arrest and senescence (Giorgi et al., 2018; Luo et al., 2011; Macip et al., 2002; Passos et al., 2010; Takahashi et al., 2006). In addition, excessive ROS causes the cleavage of collagen and elastin chains, which causes the onset of skin aging (Giorgi et al., 2018). Thus, strategies to lower ROS levels have been proposed to effectively treat aging (Lee et al., 2023). Nonetheless, physiological levels of ROS function as mediators of secondary signaling molecules in developmental processes (Sinenko et al., 2021). In particular, within the physiological concentration range, ROS reversibly oxidizes protein targets, thereby regulating stress responses and cellular metabolism (Jones and Sies, 2015). Furthermore, ROS within the physiological level provokes adaptive responses that enhance endogenous antioxidant defenses, mitigate oxidative damage over time, and increase overall stress tolerance (Ristow and Zarse, 2010). The discovery that physiological levels of ROS regulate mitohormesis, an adaptive response that extends lifespan, further supports the significance of physiological levels of ROS (Ristow and Schmeisser, 2014). In this study, we identified a novel mechanism by which dehydroacteoside reduces mitochondrial ROS by enhancing the effectiveness of OXPHOS. However, given the role of ROS-dependent signaling pathways, caution should be used when using dehydroacteosides, as reducing ROS levels below physiological levels can result in a variety of adverse effects.

5. Conclusion

In conclusion, we found that dehydroacteoside effectively reduces the amount of ROS in mitochondria of senescent fibroblasts. The effect of dehydroacteoside in reducing ROS restores mitochondrial function and rejuvenates senescence-associated phenotypes. In addition, downregulation of *TVP23C-CDRT4* was the fundamental mechanism by which dehydroacteoside rejuvenates senescence. This mechanism was further supported by the finding that *TVP23C-CDRT4* knockdown induced similar effects to dehydroacteoside. Our findings provide a novel mechanism for how dehydroacteoside rejuvenates senescence. These findings might be a potential strategy for the therapeutics to treat aging and aging-related diseases.

CRediT authorship contribution statement

Yoo Jin Lee: Writing – review & editing, Writing – original draft, Investigation, Conceptualization. **Eun Seon Song:** Writing – review & editing, Writing – original draft, Investigation, Conceptualization. **Yun Haeng Lee:** Writing – review & editing, Validation, Investigation, Conceptualization. **Kyeong Seon Lee:** Validation, Investigation. **Byeonghyeon So:** Validation, Investigation. **Ji Ho Park:** Validation, Methodology, Investigation. **Jee Hee Yoon:** Validation, Methodology, Investigation. **Duyeol Kim:** Methodology, Investigation. **Minseon Kim:** Validation, Methodology, Investigation. **Hyung Wook Kwon:**

Supervision, Formal analysis, Data curation. **Youngjoo Byun:** Writing – review & editing, Writing – original draft, Supervision. **Ki Yong Lee:** Writing – review & editing, Writing – original draft, Supervision, Conceptualization. **Joon Tae Park:** Writing – review & editing, Writing – original draft, Supervision, Conceptualization.

Ethical approval

All authors declare that all experiments were reviewed and approved by Incheon National University.

Declaration of competing interest

The authors have declared no conflicts of interest. The funders had no part in data collection, analysis, or interpretation; article writing; or decision to publish the paper.

Acknowledgments

This research was supported by a grant of the Korea Health Technology R&D Project through the Korea Health Industry Development Institute (KHIDI), funded by the Ministry of Health and Welfare, Republic of Korea (HP23C0024) and the National Research Foundation of Korea grants funded by the Korean Government (NRF-2021R1A2C1093814).

Appendix A. Supplementary data

Supplementary data to this article can be found online at https://doi.org/10.1016/j.exger.2025.112800.

Data availability

The paper includes the original contributions provided in the study. For further information, please contact the corresponding authors.

References

Adachi, H., Fujiwara, Y., Ishii, N., 1998. Effects of oxygen on protein carbonyl and aging in Caenorhabditis elegans mutants with long (age-1) and short (mev-1) life spans. J. Gerontol. A Biol. Sci. Med. Sci. 53, B240–B244.

Agar, O.T., Cankaya, I.I.T., 2020. Chapter 5 - analysis of phenylethanoids and their glycosidic derivatives. In: Sanches Silva, A., Nabavi, S.F., Saeedi, M., Nabavi, S.M. (Eds.), Recent Advances in Natural Products Analysis. Elsevier.

Bickoff, E.M., Livingston, A.L., Witt, S.C., Knuckles, B.E., Guggolz, J., Spencer, R.R., 1964. Isolation of coumestrol and other phenolics from alfalfa by countercurrent distribution. J. Pharm. Sci. 53, 1496–1499.

Boffoli, D., Scacco, S.C., Vergari, R., Solarino, G., Santacroce, G., Papa, S., 1994. Decline with age of the respiratory chain activity in human skeletal muscle. Biochim. Biophys. Acta (BBA) - Mol. Basis Dis. 1226, 73–82.

Bolden, J.E., Lowe, S.W., 2015. 15 - cellular senescence. In: Mendelsohn, J., Gray, J.W., Howley, P.M., Israel, M.A., Thompson, C.B. (Eds.), The Molecular Basis of Cancer (Fourth Edition). Content Repository Only!, Philadelphia.

Bouska, M., Huang, K., Kang, P., Bai, H., 2019. Organelle aging: lessons from model organisms. Journal of Genetics and Genomics = Yi chuan xue bao. 46, 171–185.

Byun, H.O., Jung, H.J., Seo, Y.H., Lee, Y.K., Hwang, S.C., Hwang, E.S., Yoon, G., 2012. GSK3 inactivation is involved in mitochondrial complex IV defect in transforming growth factor (TGF) β1-induced senescence. Exp. Cell Res. 318, 1808–1819.

Byun, H.O., Jung, H.J., Kim, M.J., Yoon, G., 2014. PKCδ phosphorylation is an upstream event of GSK3 inactivation-mediated ROS generation in TGF-β1-induced senescence. Free Radic. Res. 48, 1100–1108.

Castro, C.C., Vizuete, A., Deniz, B.F., Wyse, A., Netto, C.A., 2025. Sex-specific cognitive benefits and anti-inflammatory effects of coumestrol pretreatment in transient global cerebral ischemia. Mol. Cell. Neurosci. 132, 103991.

Checa, J., Aran, J.M., 2020. Reactive oxygen species: drivers of physiological and pathological processes. J. Inflamm. Res. 13, 1057–1073.

Cho, H.-J., Hwang, J.-A., Yang, E.J., Kim, E.-C., Kim, J.-R., Kim, S.Y., Kim, Y.Z., Park, S. C., Lee, Y.-S., 2022. Nintedanib induces senolytic effect via STAT3 inhibition. Cell Death Dis. 13, 760.

Choi, Y.J., Wu, X., Lee, S., Pyo, J.S., Cho, J., Cao, S., Kang, K.S., 2025. Protective effects of methylnissolin and methylnissolin-3-O-β-d-glucopyranoside on TNF-α-induced inflammation in human dermal fibroblasts. Toxicol. in Vitro 104, 106005.

Choksi, K.B., Boylston, W.H., Rabek, J.P., Widger, W.R., Papaconstantinou, J., 2004. Oxidatively damaged proteins of heart mitochondrial electron transport complexes. Biochim. Biophys. Acta 1688, 95–101.

Choksi, K.B., Nuss, J.E., Deford, J.H., Papaconstantinou, J., 2008. Age-related alterations in oxidatively damaged proteins of mouse skeletal muscle mitochondrial electron transport chain complexes. Free Radic. Biol. Med. 45, 826–838.

Dickinson, B.C., Srikun, D., Chang, C.J., 2010. Mitochondrial-targeted fluorescent probes for reactive oxygen species. Curr. Opin. Chem. Biol. 14, 50–56.

Giorgi, C., Marchi, S., Simoes, I.C.M., Ren, Z., Morciano, G., Perrone, M., Patalas-Krawczyk, P., Borchard, S., Jędrak, P., Pierzynowska, K., Szymański, J., Wang, D.Q., Portincasa, P., Węgrzyn, G., Zischka, H., Dobrzyn, P., Bonora, M., Duszynski, J., Rimessi, A., Karkucinska-Wieckowska, A., Dobrzyn, A., Szabadkai, G., Zavan, B., Oliveira, P.J., Sardao, V.A., Pinton, P., Wieckowski, M.R., 2018. Mitochondria and reactive oxygen species in aging and age-related diseases. Int. Rev. Cell Mol. Biol. 340, 209–344.

González-Gualda, E., Baker, A.G., Fruk, L., Muñoz-Espín, D., 2021. A guide to assessing cellular senescence in vitro and in vivo. FEBS J. 288, 56–80.

Hanna, R.A., Quinsay, M.N., Orogo, A.M., Giang, K., Rikka, S., Gustafsson Å, B., 2012. Microtubule-associated protein 1 light chain 3 (LC3) interacts with Bnip3 protein to selectively remove endoplasmic reticulum and mitochondria via autophagy. J. Biol. Chem. 287, 19094–19104.

Henderson, L.M., Chappell, J.B., 1993. Dihydrorhodamine 123: a fluorescent probe for superoxide generation? Eur. J. Biochem. 217, 973–980.

Hosokawa, H., Ishii, N., Ishida, H., Ichimori, K., Nakazawa, H., Suzuki, K., 1994. Rapid accumulation of fluorescent material with aging in an oxygen-sensitive mutant mev-1 of Caenorhabditis elegans. Mech. Ageing Dev. 74, 161–170.

Hwang, E., Yoon, G., Kang, H., 2009. A comparative analysis of the cell biology of senescence and aging. Cell. Mol. Life Sci. 66, 2503–2524.

Ichimura, H., Parthasarathi, K., Quadri, S., Issekutz, A.C., Bhattacharya, J., 2003. Mechano-oxidative coupling by mitochondria induces proinflammatory responses in lung venular capillaries. J. Clin. Invest. 111, 691–699.

Ilie, O.D., Ciobica, A., Riga, S., Dhunna, N., McKenna, J., Mavroudis, I., Doroftei, B., Ciobanu, A.M., Riga, D., 2020. Mini-review on lipofuscin and aging: focusing on the molecular interface, the biological recycling mechanism, oxidative stress, and the gut-brain axis functionality. Medicina (Kaunas). 56 (626).

Jones, D.P., Sies, H., 2015. The redox code. Antioxid. Redox Signal. 23, 734–746.

Kang, H.T., Park, J.T., Choi, K., Kim, Y., Choi, H.J.C., Jung, C.W., Lee, Y.-S., Park, S.C., 2017. Chemical screening identifies ATM as a target for alleviating senescence. Nat. Chem. Biol. 13, 616–623.

Kauffman, M.E., Kauffman, M.K., Traore, K., Zhu, H., Trush, M.A., Jia, Z., Li, Y.R., 2016. MitoSOX-based flow cytometry for detecting mitochondrial ROS. React Oxyg Species (Apex). 2, 361–370.

Kim, J.W., Kuk, M.U., Choy, H.E., Park, S.C., Park, J.T., 2019. Mitochondrial metabolic reprograming via BRAF inhibition ameliorates senescence. Exp. Gerontol. 126, 110691.

Kim, Y.H., Lee, Y.-K., Park, S.S., Park, S.H., Eom, S.Y., Lee, Y.-S., Lee, W.J., Jang, J., Seo, D., Kang, H.Y., Kim, J.C., Lim, S.B., Yoon, G., Kim, H.S., Kim, J.-H., Park, T.J., 2023. Mid-old cells are a potential target for anti-aging interventions in the elderly. Nat. Commun. 14, 7619.

Kohda, H., Tanaka, S., Yamaoka, Y., Yahara, S., Nohara, T., Tanimoto, T., Tanaka, A., 1989. Studies on lens-aldose-reductase inhibitor in medicinal plants. II. Active constituents of *Monochasma savatierii* Franch. et Maxim. Chem. Pharm. Bull. 37, 3153–3154.

Korkina, L.G., 2007. Phenylpropanoids as naturally occurring antioxidants: from plant defense to human health. Cell. Mol. Biol. (Noisy-le-grand) 53, 15–25.

Kuk, M.U., Park, J.Y., Song, E.S., Lee, H., Lee, Y.H., Joo, J., Kwon, H.W., Park, J.T., 2022. Bacterial artificial chromosome-based protein expression platform using the Tol2 transposon system. Biotechnol. Bioprocess Eng. 27, 344–352.

Kuk, M.U., Lee, H., Song, E.S., Lee, Y.H., Park, J.Y., Jeong, S., Kwon, H.W., Byun, Y., Park, S.C., Park, J.T., 2023. Functional restoration of lysosomes and mitochondria through modulation of AKT activity ameliorates senescence. Exp. Gerontol. 173, 112091.

Kuk, M.U., Lee, Y.H., Kim, D., Lee, K.S., Park, J.H., Yoon, J.H., Lee, Y.J., So, B., Kim, M., Kwon, H.W., Byun, Y., Lee, K.Y., Park, J.T., 2025. Sauchinone ameliorates senescence through reducing mitochondrial ROS production. Antioxidants 14, 259.

Lee, H.C., Yin, P.H., Chi, C.W., Wei, Y.H., 2002. Increase in mitochondrial mass in human fibroblasts under oxidative stress and during replicative cell senescence. J. Biomed. Sci. 9, 517–526.

Lee, Y.H., Park, J.Y., Lee, H., Song, E.S., Kuk, M.U., Joo, J., Oh, S., Kwon, H.W., Park, J. T., Park, S.C., 2021. Targeting mitochondrial metabolism as a strategy to treat senescence. Cells 10, 3003.

Lee, Y.H., Choi, D., Jang, G., Park, J.Y., Song, E.S., Lee, H., Kuk, M.U., Joo, J., Ahn, S.K., Byun, Y., Park, J.T., 2022. Targeting regulation of ATP synthase 5 alpha/beta dimerization alleviates senescence. Aging (Albany NY) 14, 678–707.

Lee, Y.H., Kuk, M.U., So, M.K., Song, E.S., Lee, H., Ahn, S.K., Kwon, H.W., Park, J.T., Park, S.C., 2023. Targeting mitochondrial oxidative stress as a strategy to treat aging and age-related diseases. Antioxidants 12, 934.

Liemburg-Apers, D.C., Willems, P.H., Koopman, W.J., Grefte, S., 2015. Interactions between mitochondrial reactive oxygen species and cellular glucose metabolism. Arch. Toxicol. 89, 1209–1226.

Luo, Y., Zou, P., Zou, J., Wang, J., Zhou, D., Liu, L., 2011. Autophagy regulates ROS-induced cellular senescence via p21 in a p38 MAPKα dependent manner. Exp. Gerontol. 46, 860–867.

Macip, S., Igarashi, M., Fang, L., Chen, A., Pan, Z.Q., Lee, S.W., Aaronson, S.A., 2002. Inhibition of p21-mediated ROS accumulation can rescue p21-induced senescence. EMBO J. 21, 2180–2188.

Mitchell, P., Moyle, J., 1967. Chemiosmotic hypothesis of oxidative phosphorylation. Nature 213, 137–139.
Miwa, S., Kashyap, S., Chini, E., von Zglinicki, T., 2022. Mitochondrial dysfunction in cell senescence and aging. J. Clin. Invest. 132, e158447.
Mookerjee, S.A., Gerencser, A.A., Nicholls, D.G., Brand, M.D., 2017. Quantifying intracellular rates of glycolytic and oxidative ATP production and consumption using extracellular flux measurements. J. Biol. Chem. 292, 7189–7207.
Muhtar, E., Ylham, G., Tiemuer, A., Edirs, S., 2024. Unraveling the dual anti-inflammatory and antioxidant mechanisms of Acteoside: computational insights and experimental validation. Chem. Biodivers., e202401564
Naik, E., Dixit, V.M., 2011. Mitochondrial reactive oxygen species drive proinflammatory cytokine production. J. Exp. Med. 208, 417–420.
Nakai, K., Tsuruta, D., 2021. What are reactive oxygen species, free radicals, and oxidative stress in skin diseases? Int. J. Mol. Sci. 22, 10799.
Neelam, Khatkar, A., Sharma, K.K., 2020. Phenylpropanoids and its derivatives: biological activities and its role in food, pharmaceutical and cosmetic industries. Crit. Rev. Food Sci. Nutr. 60, 2655–2675.
Nelson, G., Kucheryavenko, O., Wordsworth, J., von Zglinicki, T., 2018. The senescent bystander effect is caused by ROS-activated NF-κB signalling. Mech. Ageing Dev. 170, 30–36.
Nolfi-Donegan, D., Braganza, A., Shiva, S., 2020. Mitochondrial electron transport chain: oxidative phosphorylation, oxidant production, and methods of measurement. Redox Biol. 37, 101674.
Palma, F.R., He, C., Danes, J.M., Paviani, V., Coelho, D.R., Gantner, B.N., Bonini, M.G., 2020. Mitochondrial superoxide dismutase: what the established, the intriguing, and the novel reveal about a key cellular redox switch. Antioxid. Redox Signal. 32, 701–714.
Park, S., Shin, H., Park, Y., Choi, I., Park, B., Lee, K.Y., 2018. Characterization of inhibitory constituents of NO production from Catalpa ovata using LC-MS coupled with a cell-based assay. Bioorg. Chem. 80, 57–63.
Park, J.Y., Lee, H., Song, E.S., Lee, Y.H., Kuk, M.U., Ko, G., Kwon, H.W., Byun, Y., Park, J. T., 2022. Restoration of lysosomal and mitochondrial function through p38 mitogen-activated protein kinase inhibition ameliorates senescence. Rejuvenation Res. 25, 291–299.
Passos, J.F., Saretzki, G., Ahmed, S., Nelson, G., Richter, T., Peters, H., Wappler, I., Birket, M.J., Harold, G., Schaeuble, K., Birch-Machin, M.A., Kirkwood, T.B., von Zglinicki, T., 2007. Mitochondrial dysfunction accounts for the stochastic heterogeneity in telomere-dependent senescence. PLoS Biol. 5, e110.
Passos, J.F., Nelson, G., Wang, C., Richter, T., Simillion, C., Proctor, C.J., Miwa, S., Olijslagers, S., Hallinan, J., Wipat, A., Saretzki, G., Rudolph, K.L., Kirkwood, T.B.L., von Zglinicki, T., 2010. Feedback between p21 and reactive oxygen production is necessary for cell senescence. Mol. Syst. Biol. 6, 347.
Picca, A., Faitg, J., Auwerx, J., Ferrucci, L., D'Amico, D., 2023. Mitophagy in human health, ageing and disease. Nat. Metab. 5, 2047–2061.
Plitzko, B., Loesgen, S., 2018. Measurement of oxygen consumption rate (OCR) and extracellular acidification rate (ECAR) in culture cells for assessment of the energy metabolism. Bio-Protoc 8, e2850.
Poivre, M., Duez, P., 2017. Biological activity and toxicity of the Chinese herb Magnolia officinalis Rehder & E. Wilson (Houpo) and its constituents. J Zhejiang Univ Sci B 18, 194–214.
Prousek, J., 2007. Fenton chemistry in biology and medicine. Pure Appl. Chem. 79, 2325–2338.
Qi, C., Lan, H., Ye, J., Li, W., Wei, P., Yang, Y., Guo, S., Lan, T., Li, J., Zhang, Q., He, X., Wang, L., 2014. Slit2 promotes tumor growth and invasion in chemically induced skin carcinogenesis. Lab. Investig. 94, 766–776.
Quan, T., Fisher, G.J., 2015. Role of age-associated alterations of the dermal extracellular matrix microenvironment in human skin aging: a mini-review. Gerontology 61, 427–434.
Raghav, Y., Dilliott, A.A., Petrozziello, T., Kim, S.E., Berry, J.D., Cudkowicz, M.E., Vakili, K., Fraenkel, E., Farhan, S.M.K., Sadri-Vakili, G., 2024. Identification of gene fusions associated with amyotrophic lateral sclerosis. Muscle Nerve 69, 477–489.
Richards, S.A., Muter, J., Ritchie, P., Lattanzi, G., Hutchison, C.J., 2011. The accumulation of un-repairable DNA damage in laminopathy progeria fibroblasts is caused by ROS generation and is prevented by treatment with N-acetyl cysteine. Hum. Mol. Genet. 20, 3997–4004.
Ristow, M., Schmeisser, K., 2014. Mitohormesis: promoting health and lifespan by increased levels of reactive oxygen species (ROS). Dose-Response 12, 288–341.
Ristow, M., Zarse, K., 2010. How increased oxidative stress promotes longevity and metabolic health: the concept of mitochondrial hormesis (mitohormesis). Exp. Gerontol. 45, 410–418.
Senoo-Matsuda, N., Yasuda, K., Tsuda, M., Ohkubo, T., Yoshimura, S., Nakazawa, H., Hartman, P.S., Ishii, N., 2001. A defect in the cytochrome b large subunit in complex II causes both superoxide anion overproduction and abnormal energy metabolism in Caenorhabditis elegans. J. Biol. Chem. 276, 41553–41558.
Sherratt, H.S., 1991. Mitochondria: structure and function. Rev. Neurol. 147, 417–430.
Shintani, T., Klionsky, D.J., 2004. Autophagy in health and disease: a double-edged sword. Science 306, 990–995.
Sinenko, S.A., Starkova, T.Y., Kuzmin, A.A., Tomilin, A.N., 2021. Physiological signaling functions of reactive oxygen species in stem cells: from flies to man. Front. Cell Dev. Biol. 9, 714370.
Stout, R., Birch-Machin, M.A., 2019. Mitochondria's role in skin ageing. Biology 8, 29.
Sweeney, G.D., 1983. Variability in the human drug response. Thromb. Res. 29, 3–15.
Takahashi, A., Ohtani, N., Yamakoshi, K., Iida, S., Tahara, H., Nakayama, K., Nakayama, K.I., Ide, T., Saya, H., Hara, E., 2006. Mitogenic signalling and the p16INK4a-Rb pathway cooperate to enforce irreversible cellular senescence. Nat. Cell Biol. 8, 1291–1297.
Tang, Y.F., An, P.G., Gu, B.X., Yi, S., Hu, X., Wu, W.J., Zhang, J., 2023. Transcriptomic insights into adenoid cystic carcinoma via RNA sequencing. Front. Genet. 14, 1144945.
Tirichen, H., Yaigoub, H., Xu, W., Wu, C., Li, R., Li, Y., 2021. Mitochondrial reactive oxygen species and their contribution in chronic kidney disease progression through oxidative stress. Front. Physiol. 12, 627837.
Tominaga, K., Suzuki, H.I., 2019. TGF-β signaling in cellular senescence and aging-related pathology. Int. J. Mol. Sci. 20, 5002.
Turrens, J.F., 2003. Mitochondrial formation of reactive oxygen species. J. Physiol. 552, 335–344.
Van den Worm, E., Beukelman, C.J., Van den Berg, A.J.J., Kroes, B.H., Labadie, R.P., Van Dijk, H., 2001. Effects of methoxylation of apocynin and analogs on the inhibition of reactive oxygen species production by stimulated human neutrophils. Eur. J. Pharmacol. 433, 225–230.
Varani, J., Spearman, D., Perone, P., Fligiel, S.E., Datta, S.C., Wang, Z.Q., Shao, Y., Kang, S., Fisher, G.J., Voorhees, J.J., 2001. Inhibition of type I procollagen synthesis by damaged collagen in photoaged skin and by collagenase-degraded collagen in vitro. Am. J. Pathol. 158, 931–942.
Vinh, L.B., Han, Y.K., Park, S.Y., Kim, Y.J., Phong, N.V., Kim, E., Ahn, B.-g., Jung, Y.W., Byun, Y., Jeon, Y.H., Lee, K.Y., 2023. Identification of triterpenoid saponin inhibitors of interleukin (IL)-33 signaling from the roots of *Astragalus membranaceus*. J. Funct. Foods 101, 105418.
Wang, K., Klionsky, D.J., 2011. Mitochondria removal by autophagy. Autophagy 7, 297–300.
Wu, M.F., Liao, C.Y., Wang, L.Y., Chang, J.T., 2017. The role of Slit-Robo signaling in the regulation of tissue barriers. Tissue Barriers. 5, e1331155.
Wu, X., Xu, J., Cai, Y., Yang, Y., Liu, Y., Cao, S., 2021. Cytoprotection against oxidative stress by methylnissolin-3-O-β-d-glucopyranoside from Astragalus membranaceus mainly via the activation of the Nrf2/HO-1 pathway. Molecules 26, 3852.
Xiao, Y., Ren, Q., Wu, L., 2022. The pharmacokinetic property and pharmacological activity of acteoside: a review. Biomed. Pharmacother. 153, 113296.
Xu, Y., Zhang, Y., Liang, H., Liu, X., 2021. Coumestrol mitigates retinal cell inflammation, apoptosis, and oxidative stress in a rat model of diabetic retinopathy via activation of SIRT1. Aging (Albany NY) 13, 5342–5357.
Yoon, G., Kim, H.J., Yoon, Y.S., Cho, H., Lim, I.K., Lee, J.H., 2002. Iron chelation-induced senescence-like growth arrest in hepatocyte cell lines: association of transforming growth factor beta1 (TGF-beta1)-mediated p27Kip1 expression. Biochem. J. 366, 613–621.
Yoon, Y.S., Byun, H.O., Cho, H., Kim, B.K., Yoon, G., 2003. Complex II defect via down-regulation of iron-sulfur subunit induces mitochondrial dysfunction and cell cycle delay in iron chelation-induced senescence-associated growth arrest. J. Biol. Chem. 278, 51577–51586.
Yoon, Y.S., Lee, J.H., Hwang, S.C., Choi, K.S., Yoon, G., 2005. TGF beta1 induces prolonged mitochondrial ROS generation through decreased complex IV activity with senescent arrest in Mv1Lu cells. Oncogene 24, 1895–1903.
Yoon, J.E., Kim, Y., Kwon, S., Kim, M., Kim, Y.H., Kim, J.-H., Park, T.J., Kang, H.Y., 2018. Senescent fibroblasts drive ageing pigmentation: a potential therapeutic target for senile lentigo. Theranostics 8, 4620–4632.
Yoon, J.H., Kim, Y.H., Jeong, E.Y., Lee, Y.H., Byun, Y., Shin, S.S., Park, J.T., 2024. Senescence rejuvenation through reduction in mitochondrial reactive oxygen species generation by *Polygonum cuspidatum* extract: in vitro evidence. Antioxidants 13 (1110).
Zhao, R.Z., Jiang, S., Zhang, L., Yu, Z.B., 2019. Mitochondrial electron transport chain, ROS generation and uncoupling (review). Int. J. Mol. Med. 44, 3–15.
Zhavoronkov, A., Smit-McBride, Z., Guinan, K.J., Litovchenko, M., Moskalev, A., 2012. Potential therapeutic approaches for modulating expression and accumulation of defective lamin A in laminopathies and age-related diseases. J. Mol. Med. (Berl) 90, 1361–1389.
Zhou, Y., Zhu, J., Shao, L., Guo, M., 2020. Current advances in acteoside biosynthesis pathway elucidation and biosynthesis. Fitoterapia 142, 104495.
Zhu, Z., Chen, R., Zhang, L., 2024. Simple phenylpropanoids: recent advances in biological activities, biosynthetic pathways, and microbial production. Nat. Prod. Rep. 41, 6–24.
Zody, M.C., Garber, M., Adams, D.J., Sharpe, T., Harrow, J., Lupski, J.R., Nicholson, C., Searle, S.M., Wilming, L., Young, S.K., Abouelleil, A., Allen, N.R., Bi, W., Bloom, T., Borowsky, M.L., Bugalter, B.E., Butler, J., Chang, J.L., Chen, C.K., Cook, A., Corum, B., Cuomo, C.A., de Jong, P.J., DeCaprio, D., Dewar, K., FitzGerald, M., Gilbert, J., Gibson, R., Gnerre, S., Goldstein, S., Grafham, D.V., Grocock, R., Hafez, N., Hagopian, D.S., Hart, E., Norman, C.H., Humphray, S., Jaffe, D.B., Jones, M., Kamal, M., Khodiyar, V.K., LaButti, K., Laird, G., Lehoczky, J., Liu, X., Lokyitsang, T., Loveland, J., Lui, A., Macdonald, P., Major, J.E., Matthews, L., Mauceli, E., McCarroll, S.A., Mihalev, A.H., Mudge, J., Nguyen, C., Nicol, R., O'Leary, S.B., Osoegawa, K., Schwartz, D.C., Shaw-Smith, C., Stankiewicz, P., Steward, C., Swarbreck, D., Venkataraman, V., Whittaker, C.A., Yang, X., Zimmer, A. R., Bradley, A., Hubbard, T., Birren, B.W., Rogers, J., Lander, E.S., Nusbaum, C., 2006. DNA sequence of human chromosome 17 and analysis of rearrangement in the human lineage. Nature 440, 1045–1049.